national accelerator laboratory

NAL-Pub-74/38-EXP
7200.037

(Submitted to Physical Review)

INCLUSIVE PRODUCTION OF NEUTRONS IN 300-GeV pp INTERACTIONS

F. T. Dao, R. Hanft, J. Lach, E. Malamud, and F. Nezrick
Fermi National Accelerator Laboratory, Batavia, Illinois 60510

and

V. Davidson, A. Firestone, D. Lam, F. Nagy, C. Peck, and A. Sheng
California Institute of Technology, Pasadena, California 91109

and

R. Poster, P. Schlein, and W. Slater
University of California, Los Angeles, California 90024

and

A. Dzierba
Indiana University, Bloomington, Indiana 47401

July 1974

NAL-Pub-74/38-EXP
CALT-68-446
Indiana-2-74

INCLUSIVE PRODUCTION OF NEUTRONS IN 300-GeV pp INTERACTIONS*

F. T. Dao, R. Hanft, J. Lach, E. Malamud, and F. Nezrick
Fermi National Accelerator Laboratory
Batavia, Illinois 60510

and

V. Davidson, A. Firestone, D. Lam, F. Nagy, C. Peck, and A. Sheng
California Institute of Technology
Pasadena, California 91109

and

R. Poster, P. Schlein, and W. Slater
University of California†
Los Angeles, California 90024

and

A. Dzierba
Indiana University
Bloomington, Indiana 47401

ABSTRACT

An estimate of the average number of neutrons in 300-GeV pp collisions can be made from observed neutron secondary interactions (stars). The data are from a 35,000 picture exposure of the FermiLab 30-in. hydrogen bubble chamber. The average number of neutrons and anti-neutrons per inelastic collision is found to be $\langle n \rangle + \langle \bar{n} \rangle = 0.8 \pm 0.2$ and their average laboratory energy is ~ 34 GeV.

I. INTRODUCTION

There are obvious advantages and disadvantages to measuring inclusive neutron production from high-energy collisions in the bubble chamber. One has the advantage of 4π detection, but on the other hand statistics are limited because of the small probability that the neutrons will interact.

Having decided to use neutron interactions in hydrogen as our neutron detector we have to make a choice between elastic or inelastic np interactions. Elastic collisions have the advantage that once the recoil proton is measured the neutron energy is known. But using elastic collisions has several disadvantages. The probability of an elastic np collision is only ~1/4 of an inelastic collision so in this present work a sample of ~300 neutron "stars" would be replaced by only about ~75 one-prong events. Elastic events are not seen at low values of $|t|$, the four momentum transfer squared between target and recoil protons. Furthermore for high-$|t|$ a recoil proton cannot be separated from a π^+ ionization. And finally the scanning efficiency for one-prong events is low. For these reasons we have chosen to use inelastic collisions and estimate the neutron energy from the star multiplicity.

In this paper we report results on a study of inclusive production of neutrons in 300-GeV pp interactions. These results are based on a 35,000 picture exposure of the FermiLab 30-in. hydrogen bubble

chamber to a beam of 300-GeV protons. Details of the data processing have been previously reported.[1]

II. METHOD

In the complete scan, a total of 333 stars were recorded; 303 of these are in frames with at least one primary vertex, and 30 are in frames with no primary vertex.

For a partial sample the coordinates of primary and secondary vertices were measured and processed through TVGP. These coordinates are used to obtain a measurement of the angular distribution of the produced neutrons.

In order to obtain a relatively clean sample of neutron-induced events there are seven cuts and corrections we apply to the data.

1. 90° cut
2. Fiducial cut on primary vertex
3. Secondary topology cut
4. Scanning efficiency correction
5. Background subtraction
6. $K^o(\bar{K}^o)$ and Λ^o interaction subtraction
7. Secondary interaction correction

We describe each of these below and summarize the results in Table I.

1. 90° Cut. A neutron cannot be produced at a laboratory angle greater than 90° with respect to the beam. This cut reduced the sample

to 284 stars associated with 277 primary interactions. Stars at angles greater than 90° may come from $K^o(\bar{K}^o)$ interactions or from neutrals produced in secondary interactions of the charged tracks. We estimate this contamination by neutrons from secondary interactions after the 90° cut is made to be $\lesssim$ 10%.

2. Fiducial Cut on Primary Vertex. The fiducial length for the primary interaction vertex was chosen to be ~43 cm, smaller than the one used in Ref. 1 to allow enough track length for a neutron interaction. After this cut there remain 260 stars associated with 253 primary interactions.

3. Secondary Topology Cut. The scanning efficiency for one-prong stars is low. Therefore, they are removed from the sample and a model-dependent estimate of how many are expected is made below. This cut reduced the sample to 248 stars associated with 241 primary interactions and the background sample to 29 stars in pictures with no beam interactions in the hydrogen.

4. Scanning Efficiency Correction. The film has been scanned twice. The overall scanning efficiency for stars with primary vertices with the above cuts is 97%, and is 86% for stars without primary vertices.

5. Background Correction. As stated above, stars in frames without a primary vertex were recorded in order to obtain a background measurement. Twenty-nine such stars with $n_c \geq 3$ were recorded. We

assume these neutrons are created by interactions of the beam in the entrance window to the bubble chamber. Corrections for scanning efficiency, ratio of flux in photos with and without events, and fiducial volume change this background number to 30.6 events.

6. $K^{o}(\bar{K}^{o})$, Λ^{o} Interaction Correction. Neutral strange particles produced in the primary collisions also can make secondary interactions in the chamber. These strange particle-induced odd-prong stars are generally indistinguishable from neutron-induced stars except when a $K^{o}(\bar{K}^{o})$ is emitted > 90° in the laboratory .

In order to calculate this background, $K^{o}(\bar{K}^{o})$'s and Λ^{o}'s were generated by a Monte Carlo method using the measured $K^{o}(\bar{K}^{o})$, Λ^{o} momenta distributions from Phase I of this experiment,[2] using published cross sections for $K^{o}(\bar{K}^{o})$'s and Λ^{o}'s vs energy[3,4] and assuming the charged particle multiplicity distributions have a universal behavior independent of incident particle.[5,6] With the same cuts as applied to the original sample, we calculate that 56.8 $K^{o}(\bar{K}^{o})$'s and 13.4 Λ^{o}'s interact in the hydrogen and produce stars with $n_c \geq 3$. These are subtracted from the data to obtain a "pure" sample of neutrons.

7. Secondary Interaction Correction. A neutron star could be confused with a secondary interaction when the star vertex is close to a charged secondary. A correction could be calculated by Monte Carlo methods and would be a complicated function of the primary angular distribution, primary and secondary charged-particle multiplicities,

angle of the neutron, and distance to the star vertex. In a higher statistics experiment such a calculation would be warranted.

In this work we have chosen, instead, to have a physicist carefully examine a subsample of the secondary interactions (11%) on all views on a high quality, high magnification (72× film size) table. On the basis of this work it is estimated that 44±22 neutron stars were missed. This number is in addition to ~8 events already corrected for by scanning efficiency. Besides the statistical uncertainty there are many situations where it is impossible to tell if one has a secondary interaction on a charged track or a neutron star whose vertex is coincident with a charged secondary. The correction is applied as a fixed per cent to each topology although a detailed Monte Carlo calculation would probably indicate that the higher multiplicity primaries are more strongly affected.

III. RESULTS

The results are summarized in the following tables and figures: Table II shows the breakdown by secondary topology of 198.7 neutron stars. These numbers are plotted in Fig. 1 together with a fit described in the next section. The numbers in the second column of Table II are not integral because in 5% of the events the topology in the two scans differed and 1/2 event was put in each bin. The errors in the last column include the statistical errors in the events after cuts and background subtraction, and the uncertainty in the secondary interaction

correction, but do not include an uncertainty from the $K^o(\bar{K}^o)$, Λ^o correction.

Table III and Fig. 2 show the distribution of primary multiplicities for the 241 events giving rise to the 248 stars observed after cuts. It should be noted that in this figure ~2/3 of the events produce neutrons, and ~1/3 produce $K^o(\bar{K}^o)$'s and Λ^o's. The smooth curve is the multiplicity distribution (for inelastic collisions) based on 10,054 interactions reported in Ref. 1 and normalized to an area of 241 events.

Figure 3 shows a production angle distribution for a subsample of 127 stars. The variable $\eta = -\ell n \tan \theta/2$ is used. The interpretation of Fig. 3 is discussed in the next section.

IV. DISCUSSION

The produced neutrons are not monochromatic and therefore a Poisson-type distribution is not necessarily an appropriate description of the secondary prong distribution shown in Fig. 1. Nevertheless, a Poisson curve in the number of produced negatives is a convenient smooth function. A Poisson fit to the data in Fig. 1 is shown. From this fit we find $\langle n_- \rangle = 1.4 \pm 0.2$[7] the total number of neutrons, $N_T = 264 \pm 44$. This number includes the correction for the missing inelastic one-prongs.

The average potential length is 49.6 cm. This is obtained from measuring primary and secondary vertices for the 127 events whose production angle distribution is shown in Fig. 3. If we assume σ_{np}

(inelastic) is independent of neutron energy and equal to 32 mb,[8] then the weight per event is about 16.7.

Since the fiducial volume used contains 6800 inelastic collisions, $\langle n \rangle + \langle \bar{n} \rangle$, the average number of neutrons + anti-neutrons (since we do not distinguish between them) = 0.65±0.11 per inelastic pp collision. However, this number needs to be corrected for the unobserved portion of the backward hemisphere.

In contrast to Λ^o's which are observed mainly in the backward hemisphere, neutrons are observed primarily in the forward hemisphere. Forward neutrons have high laboratory energy and make high multiplicity stars. Backward neutrons have low laboratory momentum and predominantly make low multiplicity one-prong stars. For particles with $p_t >> m$, η is a good variable for separating the two hemispheres. At 300 GeV a massless particle emitted at 90° in the c.m. has θ_{lab} = 79 mrad and η = 3.2. But for a neutron p_t is smaller than m and η (90°) varies from 5.6 to 4.0 as p_t varies from 0.3 to 0.9 GeV/c. The η distributions for Λ^o's,[2] Δ^{++}'s with $|t| < 1.0 (GeV/c)^2$,[9] and neutrons are plotted in Fig. 3. For the first two of these three baryons momenta were measured, and it is known that backward hemisphere production is detected with 100% efficiency. The few forward hemisphere events have been removed. The p_t distribution of the neutrons is unknown but it is reasonable to assume it is similar to Λ^o's and Δ^{++}'s. Then the forward hemisphere neutron η distribution will be similar to the

backward hemisphere η distribution for Λ^o's and Δ^{++}'s. From these considerations it is decided to use $\eta = 4$ as an approximate dividing line between forward and backward hemisphere neutrons. Thus ~39% of the backward hemisphere is not seen in this work. This gives $\langle n \rangle + \langle \bar{n} \rangle = 0.8 \pm 0.2$, where the quoted error includes an estimate of the uncertainty in this last correction.

There is very little direct experimental information available on inclusive neutron production at high energies. Preliminary results from the ISR[10] are performed in a limited kinematic region and when integrated to obtain the total number of neutrons produced give a value lower than the one reported in this paper.

An estimate for comparison with our number can be obtained indirectly from the formula:

$$\langle n \rangle = 2 - (\langle p \rangle - \langle \bar{p} \rangle) - 2(\langle \Lambda^o \rangle - \langle \bar{\Lambda}^o \rangle) + \langle \bar{p} \rangle, \qquad (1)$$

where $\langle \Lambda^o \rangle$, $\langle \bar{\Lambda}^o \rangle$ includes $\Lambda^o(\bar{\Lambda}^o)$ from $\Sigma^o(\bar{\Sigma}^o)$, and there is an extra factor of 2 for approximate equality of Σ^+ and Λ^o although there is no experimental data on inclusive Σ^+ production at 300 GeV. Equation (1) also contains the reasonable hypothesis of approximate equality of $\langle \bar{n} \rangle$ and $\langle \bar{p} \rangle$. Data from the ISR[11] gives $\langle p \rangle = 1.30$, $\langle \bar{p} \rangle = 0.06$, and the earlier "Phase I" of our own experiment[2] gives $\langle \Lambda \rangle = 0.13$, $\langle \bar{\Lambda} \rangle = 0.01$. Thus the expected numbers are $\langle n \rangle = 0.58$, $\langle \bar{n} \rangle = 0.06$, $\langle n \rangle + \langle \bar{n} \rangle = 0.64$.

An estimate of the neutron energy is obtained from the Poisson fit shown in Fig. 1. $\langle n_- \rangle = 1.4 \pm 0.2$ corresponds to a neutron energy of 34±9 GeV.[6] As seen more clearly in Fig. 1(b) there is a high multiplicity tail which lies above the Poisson curve. If much higher statistics were available one would try to fit this distribution as the sum of two Poissons, one corresponding to (forward in c.m.) high-energy neutrons and one to (backward in c.m.) lower energy neutrons.

However, even with the limited information available in Figs. 2 and 3, it is clear that neutrons are produced near the central region and do not show the leading particle effects of protons. Figure 2 illustrates that neutrons come from a similar primary multiplicity distribution as the overall experiment. There is no enhancement for low primary multiplicity which for produced protons shows strong diffractive effects. Neutron production is slightly favored in higher multiplicity events.

The primary multiplicity distribution for Δ^{++}'s taken from Ref. 9 is also shown in Fig. 2 for comparison. Qualitatively it is similar to the distribution for neutrons except for the 4-prong enhancement caused by the diffractive process $pp \rightarrow (\Delta^{++}\pi^-)p \rightarrow (p\pi^+\pi^-)p$.

We compare our neutron result $\langle n \rangle + \langle \bar{n} \rangle = 0.8 \pm 0.2$ with an earlier result $\langle \Delta^{++} \rangle = 0.13 \pm 0.02$.[9] Since $\langle \bar{n} \rangle \approx 10\% \langle n \rangle$, the experimental ratio $\langle n \rangle / \langle \Delta^{++} \rangle \approx 6$. Consider production of neutrons and Δ^{++}'s as caused as scattering of a virtual π^- or π^+ from a proton. One can write the pole equations:

$$\left.\frac{d^2\sigma}{dt\,dm}\right|_{\pi_V^- p \to n} \xrightarrow{t \to -\mu^2} \frac{1}{4\pi m_p^2 p_L^2} \frac{G^2}{4\pi} \frac{t}{(t+\mu^2)^2} qm^2\sigma(m) \qquad (2)$$

$$\left.\frac{d^3\sigma}{dt\,dm\,dM}\right|_{\pi_V^+ p \to \Delta^{++}} \xrightarrow{t \to -\mu^2} \frac{1}{4\pi^3 m_p^2 p_L^2} \frac{1}{(t+\mu^2)^2} qm^2\sigma(m)QM^2\sigma(M) \qquad (3)$$

where m_p = proton mass, μ = pion mass, p_L = laboratory momentum corresponding to a real scattering, Q, M^2, $\sigma(M)$ are the Δ^{++} c.m. momentum, mass, and $\pi^+ p \to \Delta^{++}$ cross section, $G^2/4\pi \simeq 30$. If we integrate over the Δ^{++} parameters, ignore off-mass shell effects which will modify the t-distribution, and assume that the cross section for creating virtual pions at the other vertex is the same in both cases, then the ratio becomes:

$$\frac{\langle n \rangle}{\langle \Delta^{++} \rangle} \approx \frac{\left(\frac{G^2}{4\pi}\right) t}{\frac{1}{\pi^2}\int_{\Delta^{++}} QM^2\sigma(M)dM} \approx 4 \qquad (4)$$

for the mass and t-range for the quoted Δ^{++} cross section. Thus in the qualitative spirit in which this remark is made there is approximate agreement between the experiment and the calculated estimate.

We acknowledge the support of the FermiLab accelerator and neutrino area operations staffs and the 30-in. bubble-chamber group

during the run and the dedicated work of the staff of the FermiLab Film Analysis Facility.

REFERENCES

*Supported in part by the U. S. Atomic Energy Commission and the National Science Foundation.

†Supported in part by the National Science Foundation under grant GP-33565.

[1] A. Firestone et al., pp interactions at 300 GeV/c: Measurement of the Charged Multiplicity, Total and Elastic Cross Sections, NAL-Pub-74/37-EXP or Cal Tech Report 69-438. Submitted to Physical Review.

[2] F. T. Dao et al., Phys. Rev. Letters 30, 1151 (1973).

[3] E. Bracci et al., CERN/HERA 72-2. The average of K^+p and K^-p inelastic cross sections is used.

[4] $\Lambda^o p$ cross sections. K. Kleinknecht, Washington APS Meeting, Bull. Am. Phys. Soc. 17, 601 (1972).

[5] See, e.g., Fig. 15 in J. Whitmore, NAL-Pub-73/70-EXP or J. Lach, invited talk at the IVth International Symposium on Multiparticle Hadrodynamics, Pavia, 1973, where it is shown that $\langle n_c \rangle$ when plotted vs Q (available energy in c.m.) follows a universal curve independent of incident particle.

[6] J. Lach and E. Malamud, Phys. Letters 44B, 474 (1973). From this paper we obtain $\langle n_- \rangle = 0.84 \ell ns - 1.41$. In order to obtain $\langle n_- \rangle$ for an np, $K^o p$, or $\Lambda^o p$ collision we find an s where the available energy

$(\sqrt{s} - m_A - m_B)$ is the same as in a pp collision. The prong distribution is then taken as a Poisson distribution in the number of produced negatives.

[7] The one-prong correction can also be made using the "universal" K-N-O curve (see, e.g., A. Wroblewski, review talk presented at the Pavia Conference, September 1973). The result obtained $n_1 = 48$, agrees with the one obtained from a Poisson fit $n_1 = 65 \pm 28$ within the experimental error. The K-N-O curve also underestimates the number of high multiplicity stars.

[8] O. Benary et al., UCRL-20000 NN, August 1970, and S. P. Denisov et al., Phys. Letters 36B, 415 (1971). σ_{tot} (np or pn) = 39±1 mb over the range $10 \leq p_L \leq 60$ GeV/c. We assume $\sigma_{el} = 7$ mb.

[9] F. T. Dao et al., Phys. Rev. Letters 30, 34 (1973).

[10] J. Engler et al., paper presented at the IInd Aix-en-Provence International Conference on Elementary Particles, September 1973.

[11] M. Antinucci et al., Nuovo Cimento 6, 121 (1973).

TABLE I

Summary of Cuts and Corrections

		In Frames with Vertices	In Frames without Vertices
	Initial Sample of Events:	303	30
Cuts:	1. After $\theta_L < 90^o$ cut	284	not applicable
	2. After fiducial cut on primary vertex	260	not applicable
	3. After star multiplicity cut $n_c \geq 3$	248	29
Corrections:	4. After correction for scanning efficiency	255.5	33.8
	5. Background:		
	Correction for flux ratio, fiducial volume	-	30.6
	Difference	224.9	-
	6. After correction for $K^o(\bar{K}^o)p$, $\Lambda^o p$ interactions	154.7	-
	7. After estimate for stars missed by confusion with secondary interactions	198.7	-

TABLE II

Secondary Topology Distribution

(1) n_c	(2) Number After Cuts	(3) Corrected for Scanning Efficiency	(4) Unassociated Background	(5) Corrected for Background = (3) - (4)	(6) $K^o(\bar{K}^o), \Lambda^o$ Background	(7) Corrected for $K^o(\bar{K}^o), \Lambda^o$ = (5) - (6)	(8) Corrected for Secondary Interactions
3	119.5	123.1	11.6	111.5	31.7	79.8	102.7 ± 20.2
5	55.5	57.2	7.4	49.8	20.3	29.5	37.5 ± 13.0
7	36	37.1	4.6	32.5	10.6	21.9	28.1 ± 10.2
9	16	16.5	3.7	12.8	4.7	8.1	10.3 ± 6.7
11	10	10.3	0.6	9.7	1.9	7.8	10.1 ± 4.5
13	6	6.2	2.7	3.5	0.6	2.9	3.8 ± 3.6
15	3	3.1	-	3.1	0.3	2.8	3.7 ± 2.3
17	1	1.0	-	1.0	0.1	0.9	1.2 ± 1.2
19	1	1.0	-	1.0	-	1.0	1.3 ± 1.3
TOTAL	248	255.5	30.6	224.9	70.2	154.7	198.7 ± 33.3

TABLE III

Primary Multiplicity Distribution

n_c	$N^{(1)}$	Events Having More Than One Star[1]
2	13.5	
4	25.5	1.0[2]
6	39.5	0.5
8	45.5	0.5
10	35.5	
12	34.5	2.0
14	20.5	
16	14.0	
18	5.5	1.0
20	3.5	
22	0.5	1.0
24	1.0	
26	2.0	
TOTAL	241	7[2]

NOTES: (1) Fractional Events arise from scanning disagreement.

(2) One 4-prong event has three stars.

FIGURE CAPTIONS

Fig. 1 (a) Secondary Multiplicity Distribution. The curve, a Poisson fit to the data, is discussed in the text. (b) The same data and curve on a logarithmic scale.

Fig. 2 Primary Multiplicity Distribution for 241 events producing stars. The curve is the multiplicity distribution for all events taken from Ref. 1. The distribution for Δ^{++}'s is taken from Ref. 9.

Fig. 3 Production Angle Distribution for 127 events plotted in the variable $\eta = -\ln \tan \theta/2$. θ is the laboratory production angle. For comparison the same distribution for Λ^{o}'s (Ref. 2) and Δ^{++}'s (Ref. 9) is shown.

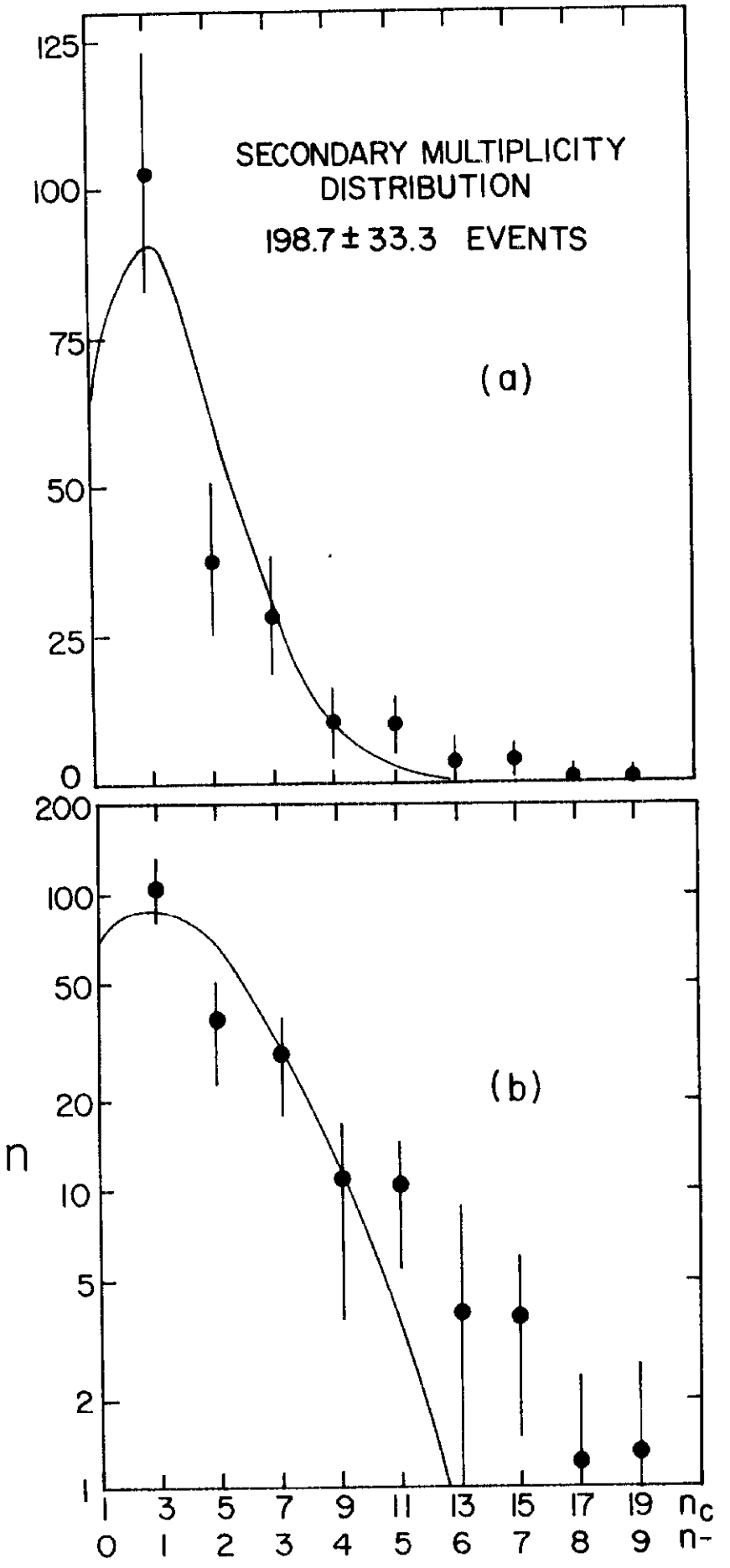
SECONDARY MULTIPLICITY DISTRIBUTION
198.7 ± 33.3 EVENTS
(a)
(b)
n
125
100
75
50
25
0
200
100
50
20
10
5
2
1
1 3 5 7 9 11 13 15 17 19 n_c
0 1 2 3 4 5 6 7 8 9 n_-

Fig. 1

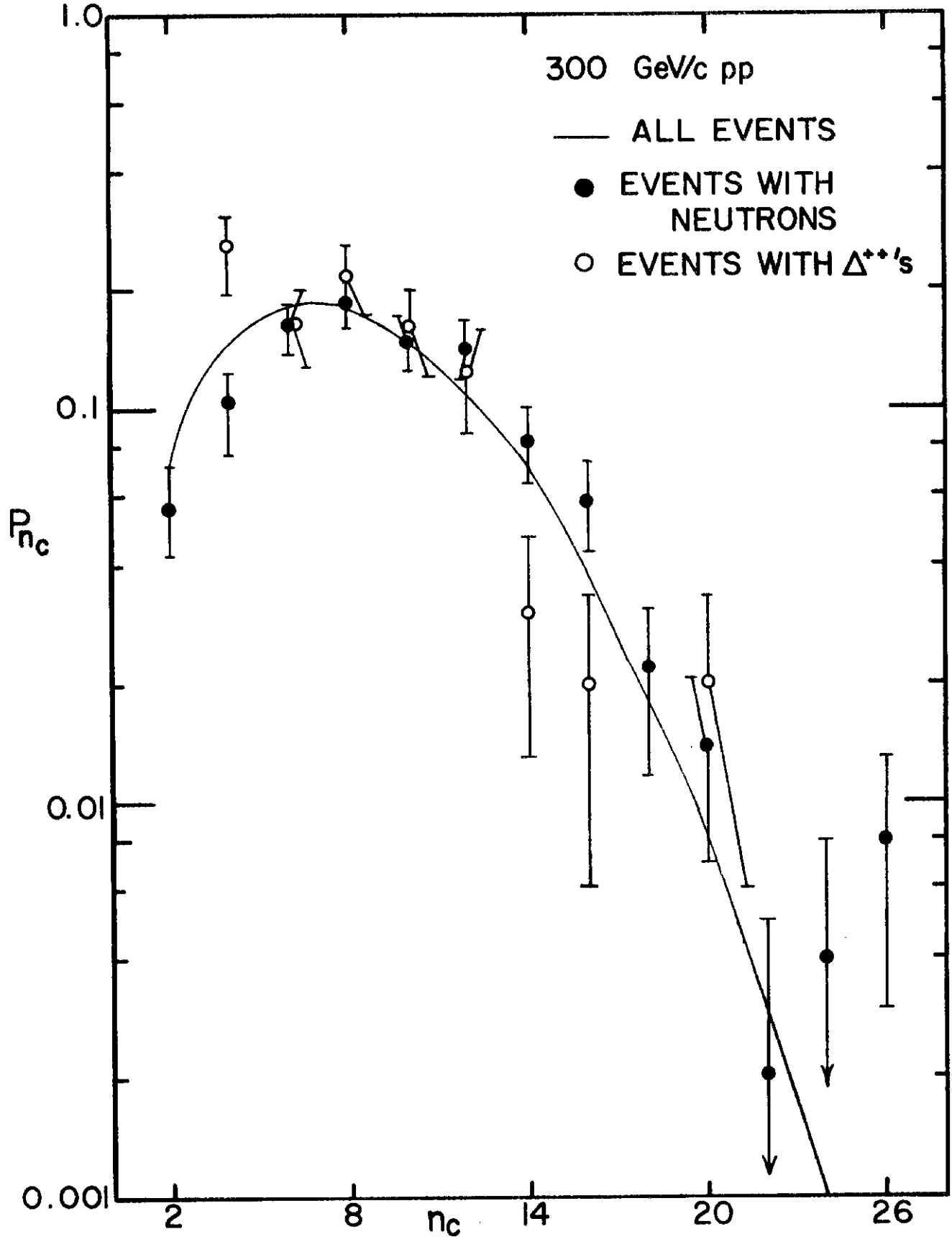
300 GeV/c pp
ALL EVENTS
EVENTS WITH NEUTRONS
EVENTS WITH Δ++'s
1.0
0.1
0.01
0.001
P_{n_c}
2
8
14
20
26
n_c

Fig. 2

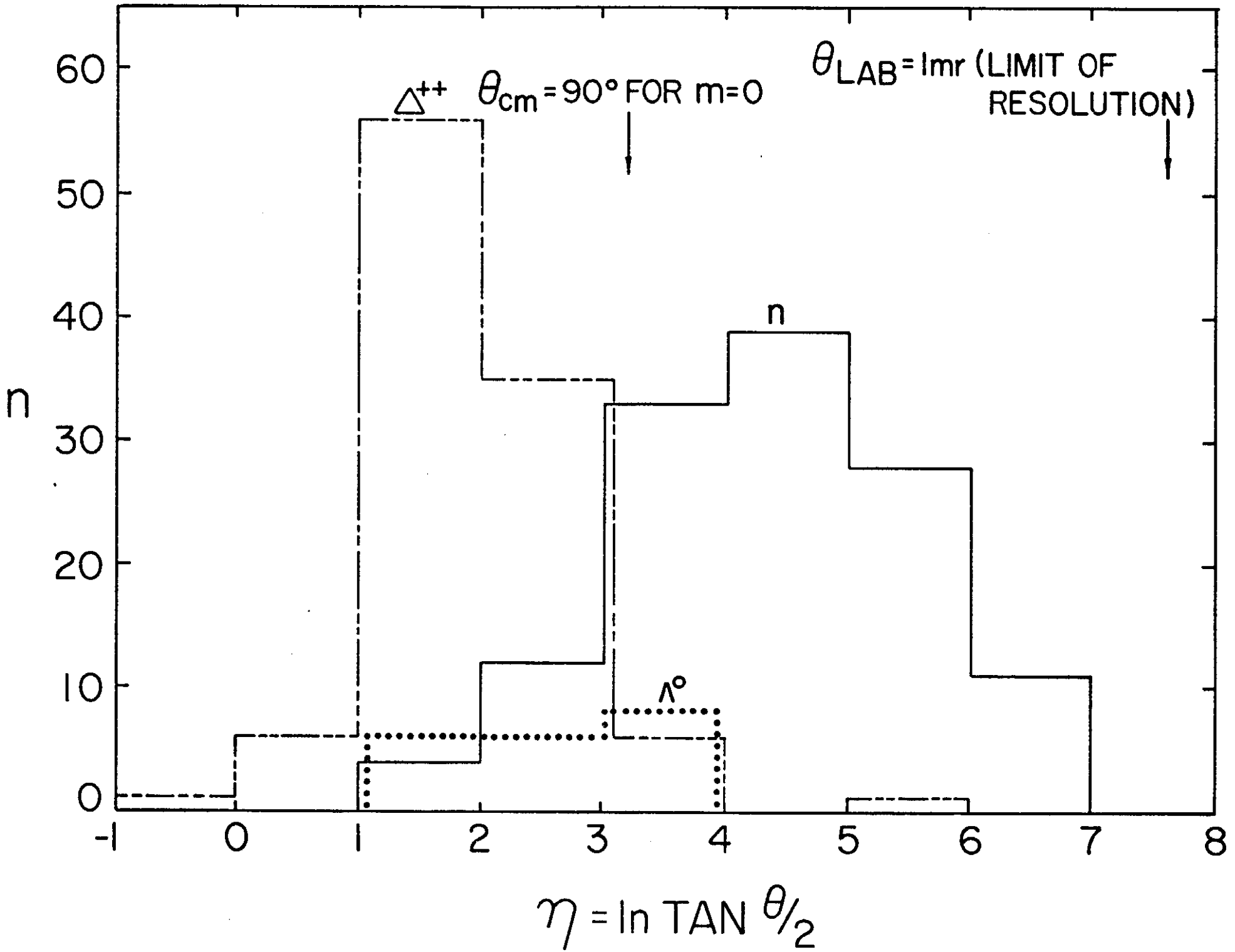
60
50
40
30
20
10
0
n
-1
0
1
2
3
4
5
6
7
8
Δ^{++}
$\theta_{cm} = 90°$ FOR m=0
θ_{LAB} = lmr (LIMIT OF RESOLUTION)
n
Λ°
$\eta = \ln \mathrm{TAN}\ \theta/2$

Fig. 3